AD-A146 071 CRITICAL DYNAMICS FOR CONTINUOUS RAPID SOLIDIFICATION PROCESSING(U) GTE LABS INC WALTHAM MA R P ADLER ET AL. AUG 84 TR-84-815.1 N00014-82-C-0434 1/1

UNCLASSIFIED F/G 11/6 NL

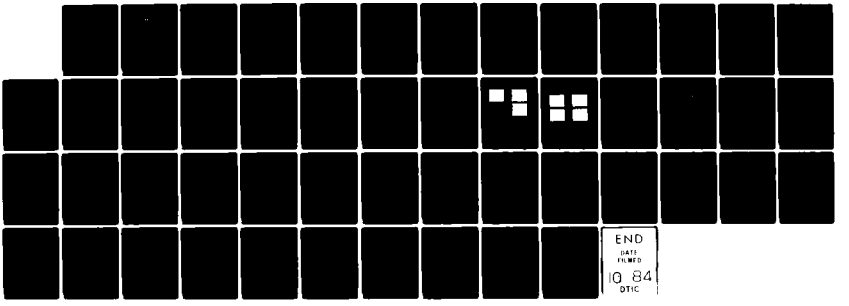

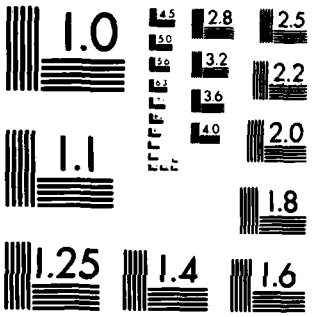

MICROCOPY RESOLUTION TEST CHART
NATIONAL BUREAU OF STANDARDS-1963-A

Research &
Development

TR 84-815.1

R|D

Critical Dynamics for Continuous Rapid Solidification Processing

Prepared for:

Office of Naval Research
800 North Quincy Street
Arlington, VA 22217

by

R.P.I. Adler
S.C. Hsu

August 1984

GTE Laboratories Incorporated
40 Sylvan Road
Waltham, MA 02254

GTE

SECURITY CLASSIFICATION OF THIS PAGE *(When Data Entered)*

REPORT DOCUMENTATION PAGE		READ INSTRUCTIONS BEFORE COMPLETING FORM
1. REPORT NUMBER	2. GOVT ACCESSION NO. AD-A146 071	3. RECIPIENT'S CATALOG NUMBER
4. TITLE *(and Subtitle)* Critical Dynamics for Continuous Rapid Solidification Processing		5. TYPE OF REPORT & PERIOD COVERED Final Report for Period 7/83 - 7/84
		6. PERFORMING ORG. REPORT NUMBER TR 84-815.1
7. AUTHOR(s) R.P.I. Adler and S.C. Hsu		8. CONTRACT OR GRANT NUMBER(s) N0014-82-C-0434
9. PERFORMING ORGANIZATION NAME AND ADDRESS GTE Laboratories Incorporated 40 Sylvan Road Waltham, MA 02154		10. PROGRAM ELEMENT, PROJECT, TASK AREA & WORK UNIT NUMBERS
11. CONTROLLING OFFICE NAME AND ADDRESS Office of Naval Research 800 N. Quincy Street Arlington, VA 02254		12. REPORT DATE August 1984
		13. NUMBER OF PAGES 46
14. MONITORING AGENCY NAME & ADDRESS*(if different from Controlling Office)*		15. SECURITY CLASS. *(of this report)* Unclassified
		15a. DECLASSIFICATION DOWNGRADING SCHEDULE

16. DISTRIBUTION STATEMENT *(of this Report)*

Approved for public release; distribution unlimited. Reproduction in whole or in part is permitted for any purpose of the United States Government.

17. DISTRIBUTION STATEMENT *(of the abstract entered in Block 20, if different from Report)*

18. SUPPLEMENTARY NOTES

19. KEY WORDS *(Continue on reverse side if necessary and identify by block number)*

Rapid Solidification Processing, Dynamic Wetting, Transient Mass and Heat Transfer, Falling Droplet Simulation Testing, Melt Spinning, Melt Puddle Dynamics, Melt Puddle Chemistry, Variable Substrate Composition Effects Process Parameter Effects

20. ABSTRACT *(Continue on reverse side if necessary and identify by block number)*

DD FORM 1 JAN 73 1473

SECURITY CLASSIFICATION OF THIS PAGE *(When Data Entered)*

ABSTRACT

Quantitative measurements of melt puddle dynamics and the associated characteristics of continuously solidified ribbon products were made as a function of materials combinations and processing conditions. A three-phase approach was taken to separately evaluate the effects of processing parameter variations, of melt chemistry, and of substrate composition. In Phase 1 two processing parameters, the melt delivery rate and the circumferential wheel velocity, were systematically varied for metalloid solute/ nickel-base alloys with Ni-12.8 a/o B-8.3 a/o Si being the primary alloy. In Phase 2, the amount of boron in ternary Ni-metalloid alloys was varied. In Phase 3, attempts to identify alternate substrates other than copper involved the use of Ni-metalloid as well as Ni-Fe-Cr-metalloid alloy melts.

Differences in melt puddle characteristics and foil properties were found as a function of materials combinations and process conditions. Foil thickness was primarily related to the circumferential velocity of the substrate wheel. Factors that changed (usually decreased) the local heat transfer kinetics had at best a second order effect on foil thickness. Since all the alternate substrate materials had lower thermal transport properties than Cu, the puddle length would proportionately increase to accommodate the slower solidification rate. For some substrates like Al, the presence of a noticeable amount of noncontact regions at the foil/ substrate interface inhibited heat flow sufficiently that the effective heat transfer rate was much lower than that expected from aluminum which has very good thermal transport figures of merit. This in part could be attributed to the formation of a tenacious surface oxide film which both reduces heat transfer and inhibits wetting of the wheel by the melt. For melt spun Ni-base alloys, Cu still remains the material of choice for the substrate, but Fe and Cu electroplated with Ni can be used when the critical quench rate to retain the amorphous phase is not too high and the design of the quenching subsystem has adequate internal cooling to avoid a significant rise in the baseline temperature of the quenchent wheel.

There were only minimal differences in solidification kinetics between melt spun crystalline and amorphous Ni-base foils. When optimized, melt spinning is a steady state process where the major rate controlling parameters and conditions are associated with the heat and mass transfer of the melt phase.

ACKNOWLEDGMENTS

This work was sponsored by the Office of Naval Research under Contract #N00014-82-C-434. We are grateful to Dr. D. Polk, ONR Scientific Officer, and Dr. J.R. McColl, Technical Manager at GTE Labs, for their comments and discussions, and to N. Schauder and W. Allen for their technical contributions. B. Simmons' help in organizing and preparing this report was most useful. Comments and input from R.V. Raman were appreciated. Analytical support by M. Downey, G. Hamill and J. Mullins in x-ray diffraction; T. Emma and G. Robinson in metallography; and E. Jungbluth and F. Kiluk in Auger spectroscopy is appreciated. The nickel-base alloys were provided courtesy of GTE Wesgo.

TABLE OF CONTENTS

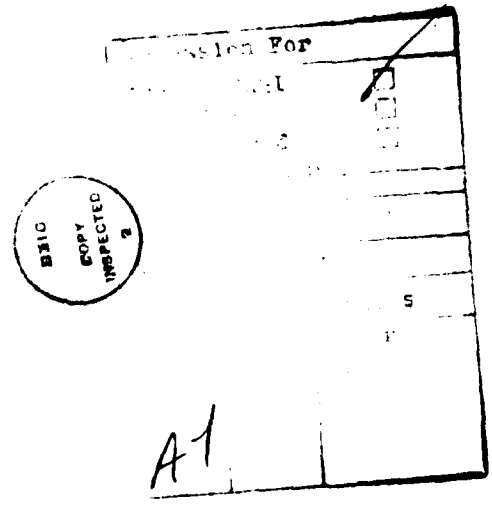

LIST OF ILLUSTRATIONS

LIST OF TABLES

1. INTRODUCTION

Melt spinning of rapidly solidified thin foil or ribbon is emerging as a high productivity process that has made the transition from the laboratory to the factory.[1–7] Especially for a specific class of materials, primarily the Group VIII transition metal-metalloid alloys, single roller chill block melt spinning (CBMS) appears to be a deceptively simple process. As long as the CBMS system is run within a finite window of processing variables, continuous, uniform product of high quality can be formed literally in a one-step operation.

The basic elements of CBMS (Figure 1) involve: the consistent delivery of a stream of metal onto a rotating heat absorbing substrate; on impact with the substrate, the liquid spreads and forms a macroscopically stationary melt puddle; material from the melt is continuously solidified at the bottom of the puddle on the moving substrate; a continuous foil product is thus simultaneously translated away from the puddle and subsequently released from the substrate wheel. When operating effectively there is a dynamic mass balance between the incoming liquid and the thin rapidly moving foil involving both heat and mass transfer. Momentum and surface energy forces of the three interacting components: (1) the liquid metal, (2) the substrate, and (3) the ambient gases, also influence puddle shape and the nature and extent of the melt/substrate contact interface.

A number of workers have attempted to model this process[8–16] and some have developed empirical relations between process variables and product characteristics and dimensions.[1, 8, 10–13, 17–23] Since the melt puddle acts as a reservoir from which the foil products are solidified, it was recognized that the shape and dimensional stability of this puddle could affect product dimensions[5, 7, 8, 11–15, 17, 19, 22–26] and many perturbations could degrade edge and surface features.[2, 5, 7, 8, 12, 13, 15, 17–19, 23, 24, 26–32] Methods to stabilize or constrain puddle shapes have also been demonstrated using mechanical[5, 7, 12, 18, 19, 33] or aerodynamic[13, 25, 27, 28] means.

Fewer attempts to correlate puddle dynamics and features with product dimensions and quality have been published.[11, 17, 18, 26, 34] This prior experimental work has been useful but may not represent steady state melt spinning conditions unless large charges (>100 gm) and an internally water cooled

substrate wheel was used. Accordingly, the methodology of this research was to systematically evaluate puddle dynamics from start to steady state conditions in order to relate these observations with material properties and process conditions. The overall goal was to use this information to provide guidelines for the selection of process parameters and materials for the melt spinning of useful rapidly solidified products.

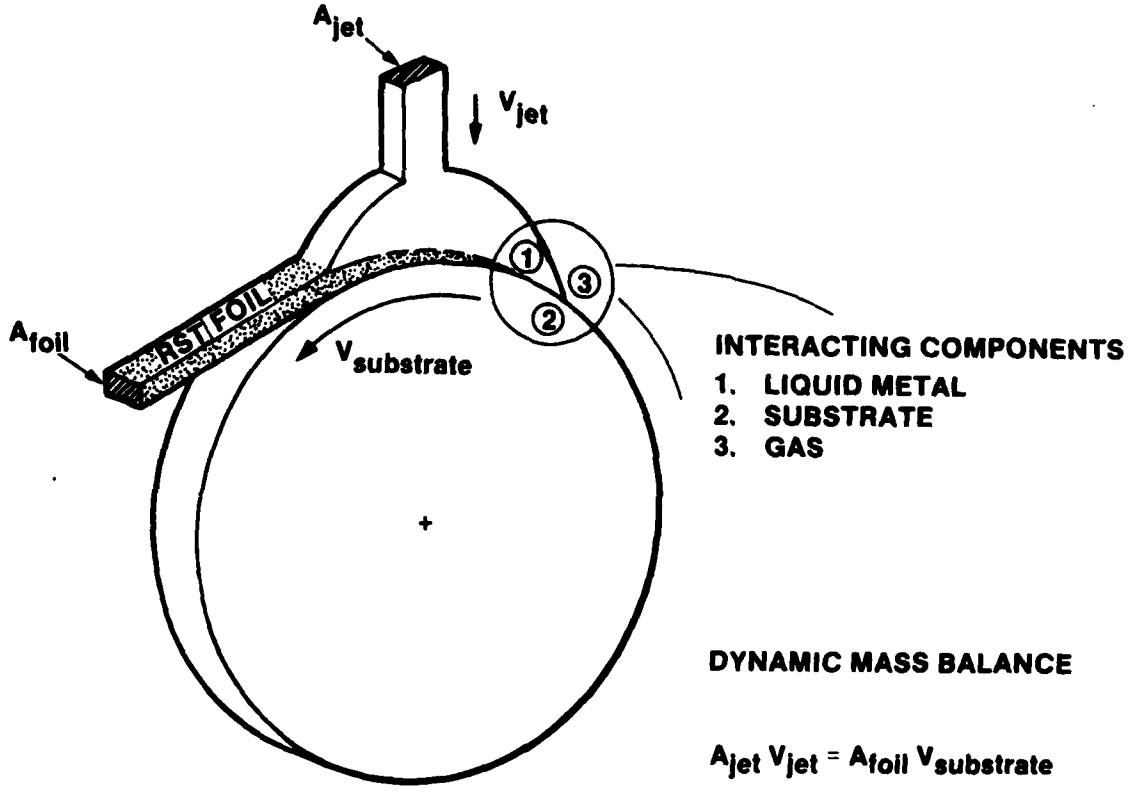

Figure 1. Essential Elements and Interacting Components for Chill Block Melt Spinning

2. REVIEW OF PRIOR CONTRACTUAL WORK

The basic objective during the first year of this study was to systematically investigate the dynamic wetting interaction for a range of melt and substrate materials. A standardized simulation test, the Falling Droplet/Inclined Substrate Plane (FD/ISP), was developed to replicate the dynamic wetting and solidification behavior during melt spinning but where all process variables were reproducible. In its simplest elements a fixed volume, molten droplet (of a candidate melt material) falls a fixed distance before it impacts against an inclined plane of a candidate substrate material. This transient thermal and mass flow phenomena is affected by the materials used while the inclined plane angle (the only process parameter varied) also produces systematic dimensional changes. The impact/spreading/wetting/retraction behavior was analyzed from high speed cinematography and along with sample characterization provided some useful insights into the important elements of melt spinning.

Most experiments used droplets from a group of metals (especially the Ni-base alloys) with a wide range of melting temperatures and surface energies impacting onto freshly prepared OFHC copper coupons. The initial momentum dominated impact and spreading phenomena produced elongated liquid discs whose maximum width extensions for any given inclination angle were the same for all metals. With increasing substrate inclination angle (θ), a more elongated, narrower and thinner disc formed. All values fell within a narrow (10%) scatter band that was inversely proportional to $\sin\theta$. When spreading stopped, surface energy forces caused different degrees and kinds of retraction and wetting. Partial retraction with simultaneous solidification resulted in splat formation -this combination of materials that caused this behavior were labeled as a wetting class. Complete retraction resulted in droplet recollection and movement away from the impact site - this behavior was characteristic of the nonwetting class.

For the nonwetting class such as a Ni-20 Cr droplet on a Cu substrate, droplet reformation occurred at all inclination angles. With little tendency to wet the substrate, minimal heat transfer occurred and splat solidification was avoided. Such combinations were predicted to be characteristic of difficult to melt spin systems because minimal contact between the melt puddle and

the substrate would inhibit adequate heat transfer and thus uniform, rapidly solidified foil would be difficult to form during melt spinning.

For the wetting combination, the degree of contact between the melt and the substrate is greater and more intimate thus favoring high heat transfer rates and the formation of solidified splats at all angles. For any material there will be a systematic difference between the final solidified width and the maximum extension of the liquid film which should be proportional to surface energy driven retraction forces. Metals such as Cu, Zr, Al, Ni and four binary Cu-Ni alloys exhibited wetting behavior. For all the Cu-Ni alloy series a single curve with minimal data point scattering was sufficient to describe their behavior; thus apparently no critical bulk or surface properties pertinent to this phenomena were altered by alloying.

A third class of transitional behavior materials was identified; at low inclination angles they behaved like the nonwetting class. However as the inclination angle became steeper and the liquid film thinner, there was an abrupt transition to the splat solidification mode of the wetting class. This occurred at $\theta = 45°$ for the AMS4778 alloy and $\theta = 40°$ for a Marko 1.27 alloy (Fe-15% Cr-5% Ni-1% Nb-0.5% Cu-2.2% B). Since both alloys can be readily melt spun this type of transitional behavior may be representative of alloy systems in which wetting and heat transfer do occur but where the bonding of the solidified material with the substrate is not too strong to permit foil release.

Melt spinning correlation runs were then conducted with Cu and Ni-base alloy melts representative of the three classes of behavior. The transitional AMS4778 alloy formed an oscillating human-foot shaped melt puddle from which the best quality foil forms and will be elaborated on more completely subsequently.

In contrast a copper melt/copper substrate wheel combination representative of the wetting class produced a wildly oscillating puddle with a very small footprint that produced a low integrity, discontinuous product. For the other Ni-base wetting combination (80 Ni-20 Cu) complications related to its higher melting point required some experimental modification to produce jet flow. Air melt spinning produced a semicontinuous (up to several feet long), low quality fiber. Typical foils had longitudinally varying widths in the range of 0.060 ± 0.020 in. The longitudinally striated free surface often had

a pattern of massive or elongated through-thickness voids and edge slivers that can be associated with a spreading fluid flow pattern. This effect appears to be due to formation of lift-off voids, which normally form on the contact surface but are larger than normal in this case, that grow and emerge through the foil. This may be associated with low liquid viscosity during solidification. The product morphology and quality matches that of melt spun pure copper, consistent with previously reported melt drop results for the binary Cu-Ni system.

For the nonwetting example, 80 Ni-20 Cr, some modifications to the usual melt spinning practice was also needed to produce jet flow. The resultant product was oxidized and discontinous. Most of the foil produced was short (2 in. average length) and narrow (0.03 in.). The mechanical breakup of the original product occurred either during solidification or subsequent handling. The substantial width and thickness irregularities of the cross-sectional profile combined with a rounded edge definition are indicative that the foil solidifies from a dimensionally unstable melt that maintains minimal contact with the moving copper substrate.

Due to the above complications involved in air melt spinning of readily oxidizable melts that minimize wetting and thermal contact as well as practical difficulties in preparing notched bar samples from either very hard or brittle material for the FD/ISP test, further efforts at this form of simulation testing and empirical melt spinning correlations were halted. Instead a shift to a comprehensive program to investigate process and material factors that can be used to optimize the melt spinning practices for other lower melting Ni-base alloys was made and forms the bulk of the report on this years work. More complete details of this earlier 1983-84 effort have been covered in the September 1983 Annual Report for this Contract N00014-82-C-0434 and extra copies are available on request.

3. GENERAL EXPERIMENTAL PROCEDURES

In order to achieve our goal of effectively identifying which hydrodynamic and material properties are significant to the melt spinning process, a well calibrated facility with a standardized experimental procedure was used at GTE Labs. The melt delivery subsystem consisted of a sealed quartz pressure vessel having an orifice disc with a 1 mm diameter passage in the bottom. This orifice was located directly above the top dead center of an internally water cooled, 20.3 cm diameter melt quenching wheel. A fixed orifice to substrate distance of 1.35 cm was consistently maintained to facilitate viewing.

The melt spinning procedure consists of inductively heating a prealloyed charge of at least 100 gm under a light flow of forming gas (95% N_2-5% H_2) in the melt delivery vessel. Upon reaching the 100°C superheat (measured with a quartz sheathed thermocouple immersed in the melt), the rotating substrate is brought up to the desired speed and then additional forming gas is quickly admitted to establish a desired overpressure level which forces the melt through the orifice forming a stable jet in air. The jet flow direction is perpendicular to the outer cylindrical surface of the quenchant wheel which is continuously dressed by a counter rotating abrasive tape flapper wheel device. On impact the jet spreads and typically forms a human-foot shaped puddle. The longitudinal, side view profile of this unencumbered melt puddle is photographed at 1000 frames per second with a Redlake Hycam high speed (rotating prism and continuously moving film) motion picture camera.

Each film with over 6000 frames provided a record of puddle dynamics for evaluation. Typically quantified measurements of puddle length and height were made from 100 to 150 systematically chosen frames. Because the puddle was somewhat larger and typically more unstable during the initial substrate revolution than for subsequent rotations, most listed puddle characterization measurements are statistical averages with the associated two standard deviation values from data taken after the initial substrate rotation but during the first three seconds of operation. During this period the melt mass flow rate and the baseline temperature of the rotating substrate usually stabilize. Most foils were also continuous so that sequential evaluation of foil dimensions, micro/macrostructure, morphology and weight per unit length could be made and indexed with the number of wheel rotations after startup.

The choices for melt chemistry and substrate material were systematically varied according to the specific subobjectives of each of the three experimental phases of this program. In Phase 1 the emphasis was on evaluating the effects of changing process variables. Thus only three Ni-base metalloid ternary alloys were used in which the only significant changes were in the numerical values of the boron and silicon metalloid values.

In addition to using a copper wheel which is the accepted standard among melt spinning technologists, a second dimensionally identical wheel was made from molybdenum. The choice of Mo was based on its higher melting temperature, good mechanical properties, and acceptable values for either thermal figure of merit (satisfactory for relative heat absorption and good for thermal diffusivity) as listed in Table 1. Thus with a thermal diffusivity about 65% that of Cu, Mo was expected to have enough intrinsic thermal capacity to get the sensible heat given up by the melt into the internally circulating coolant loop. Also the higher surface energy ratio for Mo (Table 1) suggested that other factors being equal, Mo is more likely to be wetted by a metallic melt than the other candidates. This in turn could affect the nature of the dynamic substrate/melt interaction.

In Phase 2 the emphasis was on evaluating what changes in metalloid levels had on product and process characteristics. The baseline composition was the Ni-base ternary deep eutectic AMS4778 alloy (with 12.8 atomic percent (a/o) B and 8.3 a/o Si). Essentially only changes in the boron content from 1.8 a/o to 14.4 a/o were made. All process conditions were fixed and only the standard water cooled copper substrate was used.

In Phase 3, the effects of alternate substrate materials were evaluated. In addition to using two available Cu and Mo wheels, prototype one half inch wide circular plates of the standard circumferential dimension were fabricated with provisions for internal water cooling from 1040 steel, 2024 aluminum, and copper that had either a thin (~0.004 in.) electroplated coating of Cr or Ni. In addition a limited array of commonly available ternary Ni-base/metalloid brazing alloys and a fourth Ni-base alloy AMS4777 (with 14.0 a/o B, 7.1 a/o Si, 2.7 a/o Fe and 6.7 a/o Cr) were used. In the latter case, to examine whether the presence of common elements in both the melt and on the substrate surface can affect the dynamic wetting process.

TABLE 1

THERMAL AND PHYSICAL PROPERTIES OF SUBSTRATES

MATERIAL	MELTING POINT (°C)	PROPERTIES RELATIVE TO COPPER		
		SURFACE ENERGY	HEAT ABSORPTION	THERMAL DIFFUSIVITY
Cu	1083	1.0	1.0	1.0
Ni on Cu	1452	1.5	1*	1*
Cr on Cu	1875	1.6	1*	1*
Al	660	0.62	0.40	0.80
Fe	1536	1.31	0.20	0.19
Mo	2610	2.08	0.20	0.65

Heat Absorption = $K\varrho\ C_p$

Thermal Diffusivity = $K/\varrho\ C_p$

Where: K is the Thermal Conductivity
ϱ is Density
C_p is Specific Heat

* Neglect Effect of Thin Electroplated Layer on Bulk Thermal Characteristics of Copper

4. CURRENT ACTIVITIES

4.1 PHASE 1: EVALUATION OF SYSTEMATIC CHANGES IN PROCESS VARIABLES

4.1.1 Objectives and Special Conditions

The objective of this phase of the program was to examine how systematic changes in some processing variables affect other process and product characteristics.

The choices for melt chemistry and substrate material were based on evaluating whether differences in thermal and physical properties are significant. Two commercially available ternary nickel-base brazing alloys with only numerical differences in their boron and silicon metalloid values were selected. The higher metalloid content alloy (with 12.8 a/o and 8.3 a/o Si) designated as AMS4778 represented materials that are easy to melt spin into amorphous products. The lower metalloid content (8.7 a/o B and 6.6 a/o Si) AMS4779 alloy was chosen because it usually forms a crystalline foil when melt spun. Another alloy designated AMS4778-low B (9.4 a/o B and 8.2 a/o Si) that forms a partly crystalline product was also used for comparative purposes.

Only the standard Cu substrate wheel and a dimensionally similar one made from Mo were used since these two materials had a reasonable spread in their thermal figures of merit and surface energies (Table 1). Care was taken to determine if such differences could produce changes in the nature of the dynamic wetting process or product characteristics.

Several changes in both wheel speed and melt overpressure provided a limited matrix of processing conditions. Product/process comparisons were made against those from an empirically selected standard condition (1.5 psi overpressure for a Cu wheel rotating at 1500 rpm where a quality amorphous ribbon is reproducibly produced by melt spinning).

4.1.2 Results and Discussion

For each melt spinning run, foil dimensions and gravimetric values were measured and the average values of some are listed in Table 2. Foil widths were measured with a low power filar eyepiece and the average value for at least 20 readings from a meter-long sample was recorded. For comparative

purposes these averaged width values were found to be consistent with processing conditions. Perhaps the most representative and reproducible quantities were the weight per unit length (W/L) data where specific samples usually were longer than one meter. Although there were some experimentally related variation in W/L values, for any given melt/ substrate combinations decreasing rpm or melt delivery rate produced expected increases or decreases of W/L values, respectively.

TABLE 2

PROCESS AND PRODUCT CHARACTERISTICS

PARAMETERS	SYMBOL
Foil Weight per Meter (gm/m)	W/L
Mass Flow Rate (W/L · V_s) (gm/s)	dW/dτ
Foil Width (mm)	Width

ALLOY/SUBSTRATE	PARAMETER	PROCESSING CONDITIONS WITH 1mm ϕ ORIFICE		
		1000 rpm (10.64 m/s)	1500 rpm (V_s = 15.95 m/s)	
		1.5 psi	1.0 psi	1.5 psi
4778 Cu	W/L dW/dτ Widths	0.733 7.80 1.27	0.410 6.54 1.143	0.570 9.09 1.651
4778 Mo	W/L dW/dτ Widths	0.830 8.83 1.372		0.753 (0.633)* 12.01 (10.10)* 1.778 — 2.159 (1.27 — 1.651)*
4778 (Low B) Cu	W/L dW/dτ Widths			0.750 11.96 1.854
4779 Cu	W/L dW/dτ Widths	0.780 8.30 1.397	0.680 10.85 1.778	0.720 11.48 2.057

*Values at end of run.

The mass flow rate (dW/dt) of this system where all the incoming melt in the jet was converted to foil for each run was calculated from the product of

the wheel velocity and the W/L value. When the width is plotted as a function of this mass flow rate for all runs (Figure 2), a distinct relationship is present. Furthermore since the diameter of the orifice is fixed at 1 mm, there is a direct proportionality between mass flow rate and velocity. In order to determine if there was an exponential relationship between width and mass flow rate (or jet velocity in this specific case), the data was plotted on a log-log plot (not shown). Because of data scatter a reasonable value for the slope in that plot was $n = 1 \pm 0.2$. This n is the exponent for the mass flow rate (and in this case jet velocity) meaning that:

$$\text{width} = K(dW/d\tau)^n = K^*(\text{jet velocity})^n$$

This relationship appears to be reasonable and consistent with others.[8, 10, 12, 13, 20–23, 26]

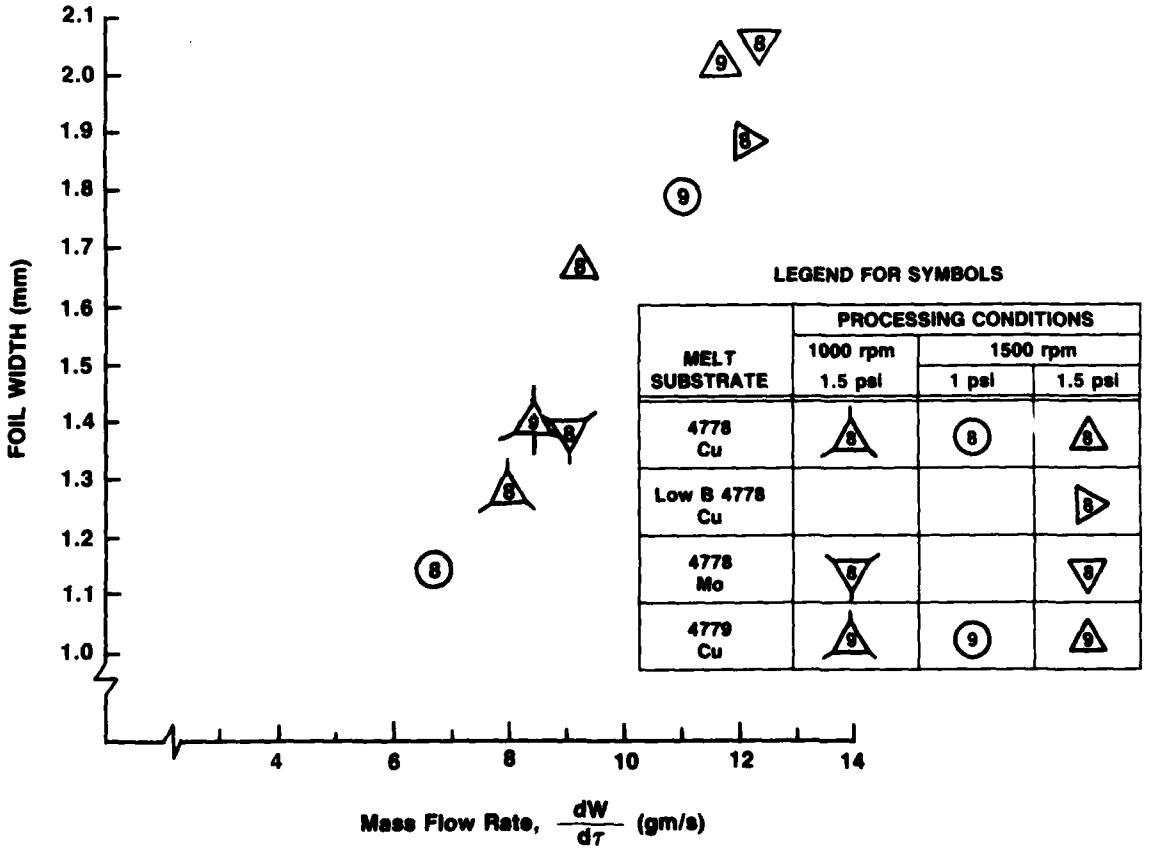

Figure 2. Foil Width/Processing Condition Correlation

Macroscopic and x-ray diffraction examination of foils revealed some interesting differences that resulted from melt spinning on either Cu or Mo wheels. Some scanning electron microscopy photos of representative free surfaces of foil samples are shown in Figure 3. In general, all AMS4778 foils melt spun on our Cu wheel are amorphous and have smooth, nearly flat free surfaces with good, nearly linear edge definition. For those melt spun on Mo wheels, even samples from the beginning of a run had slightly jagged edges but were still amorphous. This serrated edge effect becomes progressively more noticeable until at the end of the run the edges are very jagged and the transverse foil profile is quite crowned.

The jagged edges such as those on foils melt spun from Mo wheels are due to a liquid decanting type of effect which exposes the advancing solidification front. For melt spinning decanting occurs whenever heat transfer (from an initially spreading liquid metal film onto its supporting substrate) is slow enough that surface energy forces can cause the remaining (overlying) liquid to (partially) retract before it solidifies. Whether the receding film is created after a liquid droplet impacts and spreads on a substrate[35] or occurs at the edge of a melt puddle during melt spinning,[17] usually surface energy by itself is not strong enough to cause complete liquid retraction. However for melt spinning runs with our Mo wheel the continual increase in baseline temperature is due to the inability of this melt quenching subsystem to quickly pass the sensible heat from the melt puddle into the coolant at the same rate that additional heat is being added. This lower heat transfer situation systematically allows increasingly more time for partial puddle edge retraction to occur. The resultant foils become narrower (note asterisked value for the foil width from the end of the run in Table 2) with more pronounced edge features. There was a parallel rise in crystalline phase content of these foils towards the end of the run. This is to be contrasted with an equivalent melt spinning run with a Cu wheel where high quality, amorphous foils were always produced. Thus, to exploit the other advantages of using a Mo substrate (despite its lower thermal figures of merit) strict attention to the design of the overall quenching subsystem is required in order to raise the thermal transfer capabilities of all its parts.

(a) WITH Cu WHEEL REPRESENTATIVE OF ENTIRE RUN

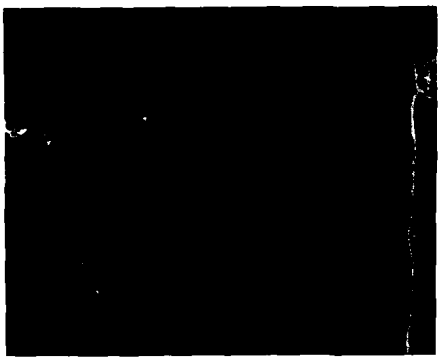

SCALE: 1 mm

FIXED PROCESS CONDITIONS

MELT DELIVERY
1 mm DIAMETER ORIFICE
1.5 psi OVERPRESSURE
MELT QUENCHING SUBSTRATE
1500 rpm
20.32 cm DIAMETER WHEEL

(a) WITH Mo WHEEL AT START OF RUN

(b) AT END OF RUN WITH Mo

Figure 3. Free Surface and Edge Morphologies of Melt Spun AMS4778 Foils

Examination of contact surfaces of AMS4778 foils revealed that each type of substrate produced distinctly different surface features (Figure 4). The contact surface of foils melt spun with a Cu wheel had an overall pattern of elevated surface ridges probably replicating the longitudinal wheel striations produced by a continuous surface dressing device. In addition a random pattern of triangular voids was present as previously reported.[29-32] For foils melt spun on a Mo wheel there was a bimodal distribution of smaller, irregularly shaped depressions and rather large, rounded surface pores superimposed on a mottled background where more intimate foil/substrate contact existed. The more rounded nature of these pores may reflect the effect of the higher surface energy and a lower solidification rate on Mo which allows more time for

some material redistribution to reduce the effective surface area. Auger analysis also showed no trace of Mo pickup on this foil contact surface, thus any Mo interactions that may cause these alterations are the result of physical rather than chemical effects.

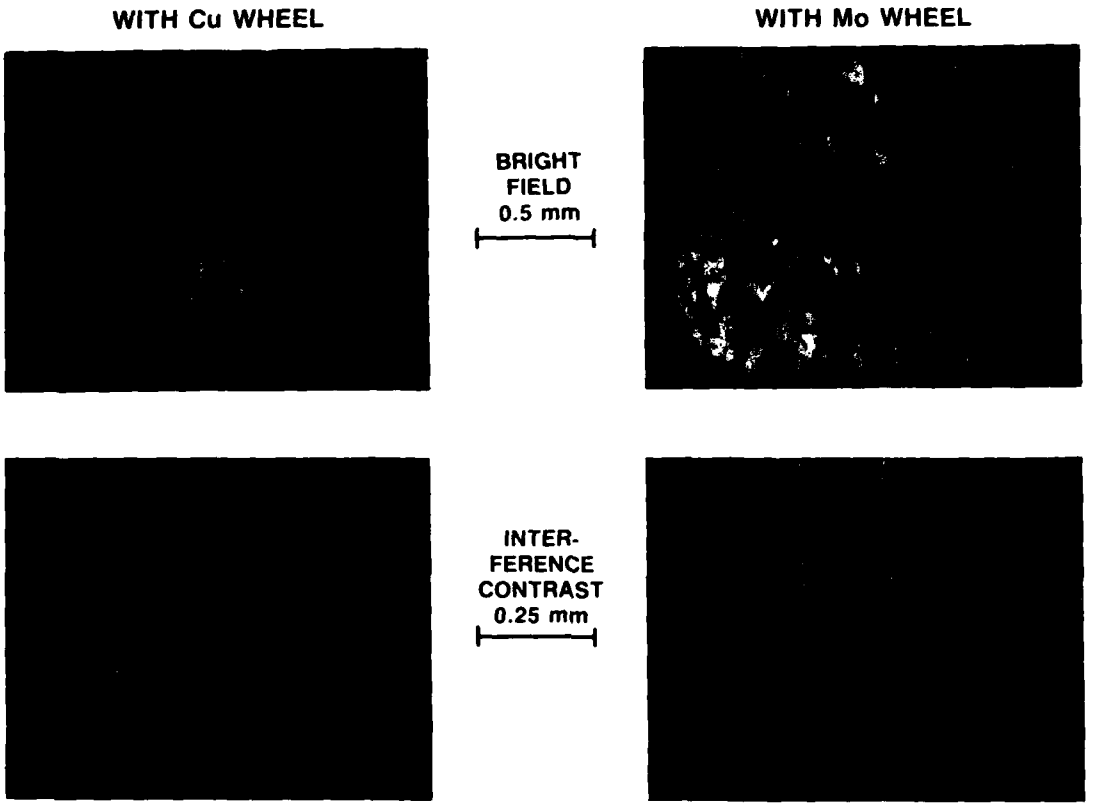

Figure 4. Contact Surface Features of AMS4778 Foils Melt Spun at 1500 rpm and 1.5 psi Overpressure

It was important to measure puddle dimensions and characteristics since these should be related to foil geometry and quality. A systematic series of movie frames were analyzed for puddle length (ℓ) and height (h) and the averaged values are presented in Table 3 along with an aspect ratio (h/ℓ) and a term proportional to the longitudinal cross-sectional area ($h \times \ell$).

Some overall observations from this and an earlier[17] study are that both the length and the height of the puddle experience significant deviations that are random in time and generally show no consistent correlation between these two dimensions. Runs where either averaged dimension is consistently large (as

quantified by the puddle aspect ratio and specifically when 1/3 <h/ℓ> 1) tend to have correspondingly larger variations. The low B alloy had comparable puddle dimensions to those for the regular AMS4778 alloy but because its mass flow rate was higher tended to have a slightly longer contact length. On the other hand the lower boron, AMS4779 alloy always had a shorter contact length than equivalent AMS4778 runs producing a puddle that appeared taller.

One general trend that results when the substrate is changed from Cu to Mo is that in all cases the puddle was significantly longer with a comparable change in the longitudinal profile area. Another processing change, reduction of the surface velocity of the substrate from 15.95 to 10.64 m/s, produces a shallower but longer puddle which appears to have a larger puddle from the $h \times \ell$ product. In fact it is usually smaller when the three-dimensional volume is calculated using the foil width dimension also. In contrast keeping substrate velocity constant at 15.95 m/s and reducing the mass flow rate by roughly 30% for the AMS4778/Cu combination and under 10% for the AMS4779/Cu combination (as a result of dropping the overpressure from 1 1/2 to 1 psi) causes moderately little change in the longitudinal puddle shape. However in both of these cases a narrower ribbon is formed where the width ratio closely matches the experimental mass flow ratios.

Some of the information in Tables 2 and 3 can be combined to calculate two useful solidification parameters in Table 4. Here the calculated thickness is a bulk averaged value that is stable (±5%) over the entire run and is a reproducibly characteristic parameter for making run to run comparisons. This value is far better than those using micrometer techniques which produce considerable data scatter and for rough foils tend to read maximum rather than average values. The other term is the residence time that a foil element can grow in thickness while under the puddle. This value is calculated from the ratio of the puddle footprint length to the substrate velocity.

Since the thickness solidified (t_c) is proportional to the square root of residence time ($\tau_R^{1/2}$) for normal solidification kinetics, our data was plotted accordingly in Figure 5. Clearly for a given rotation rate, foil thickness is nominally the same irrespective of substrate and melt composition or overpressure; meanwhile there are real differences in residence times. Three straight lines can be drawn through various substrate/melt combination data points. Each slope constant is the effective heat transfer coefficient of that

TABLE 3

MELT PUDDLE CHARACTERISTICS

PARAMETER	SYMBOL	ILLUSTRATION
Puddle Length (mm)	$\ell \pm \triangle\ell$	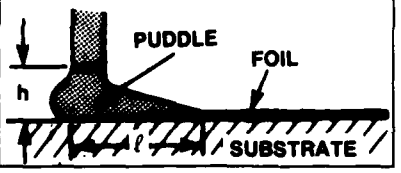
Puddle Height (mm)	$h \pm \triangle h$	

ALLOY/SUBSTRATE	PARAMETER	PROCESSING CONDITIONS WITH 1mm ϕ ORIFICE		
		1000 rpm	1500 rpm	
		1.5 psi	1.0 psi	1.5 psi
4778 Cu	ℓ	7.95 ± 2.11*	4.28 ± 0.50	3.84 ± 0.79*
	h	1.43 ± 0.31*	2.29 ± 0.35	2.79 ± 0.81*
	h/ℓ	0.18	0.53	0.73
	$h \times \ell$	11.37	9.89	10.7
4778 Mo	ℓ	11.66 ± 3.08*		6.31 ± 1.96*
	h	1.73 ± 0.50*		1.99 ± 0.78*
	h/ℓ	0.15		0.32
	$h \times \ell$	20.17		12.56
4778 (Low B) Cu	ℓ			4.39 ± 0.66
	h			1.83 ± 0.46
	h/ℓ			0.42
	$h \times \ell$			8.03
4779 Cu	ℓ	5.79 ± 1.73*	3.11 ± 0.31*	3.47 ± 0.72*
	h	1.69 ± 0.68*	2.31 ± 0.50*	2.47 ± 0.80*
	h/ℓ	0.29	0.74	0.711
	$h \times \ell$	9.79	7.18	8.58

*Indicates 2σ (σ = standard deviation) spread.

combination of materials and process conditions and is sensitive to those variables that have a second order effect on thickness. For the case of the AMS4778/Mo combination, the lower heat transfer capacity of Mo compared to Cu caused the Mo wheel to heat up during a run. This caused puddle elongation to accommodate the longer time needed for solidification. While no major differences in puddle dynamics were observed, it is apparent that crystalline AMS4779 foils grow faster than similarly processed amorphous AMS4778 material. This occurs despite the additional heat from the latent heat of fusion that must be disposed of when crystalline solidification occurs. Perhaps it is a combination of a faster growing crystalline solidification front and/or a higher heat transfer rate through its own solidified layer (when this layer is crystalline rather than amorphous) that effectively reduces the through thickness foil solidification time for AMS4779 compared to AMS4778 foils. The intermediate location of the low B AMS4778 data point between the 4779/Cu and 4778/Cu lines indicates that changes in boron content can cause small slope changes. However with only minimal differences in solidification kinetics between systems that solidify as crystalline or amorphous foils, the major rate controlling parameters and conditions in melt spinning must be associated with the heat and mass transfer of the melt phase.

TABLE 4

SOLIDIFICATION CHARACTERISTICS

PARAMETERS	SYMBOL
Residence time of substrate element under puddle (ℓ/Vs) (10^{-6} min)	τ_R
Calculated thickness (W/L ÷ width) (gm/cm^2)	t_c

ALLOY/SUBSTRATE	PARAMETER	PROCESSING CONDITIONS WITH 1mm ϕ ORIFICE		
		1000 rpm	1500 rpm	
		1.5 psi	1.0 psi	1.5 psi
4778 Cu	τ_R t_c	12.447 0.0594	4.486 0.0359	4.008 0.0346
4778 Mo	τ_R t_c	18.259 0.0606		6.589 0.0382
4778 (Low B) Cu	τ_R t_c			4.580 0.0404
4779 Cu	τ_R t_c	9.060 0.0583	3.244 0.0393	3.610 0.0348

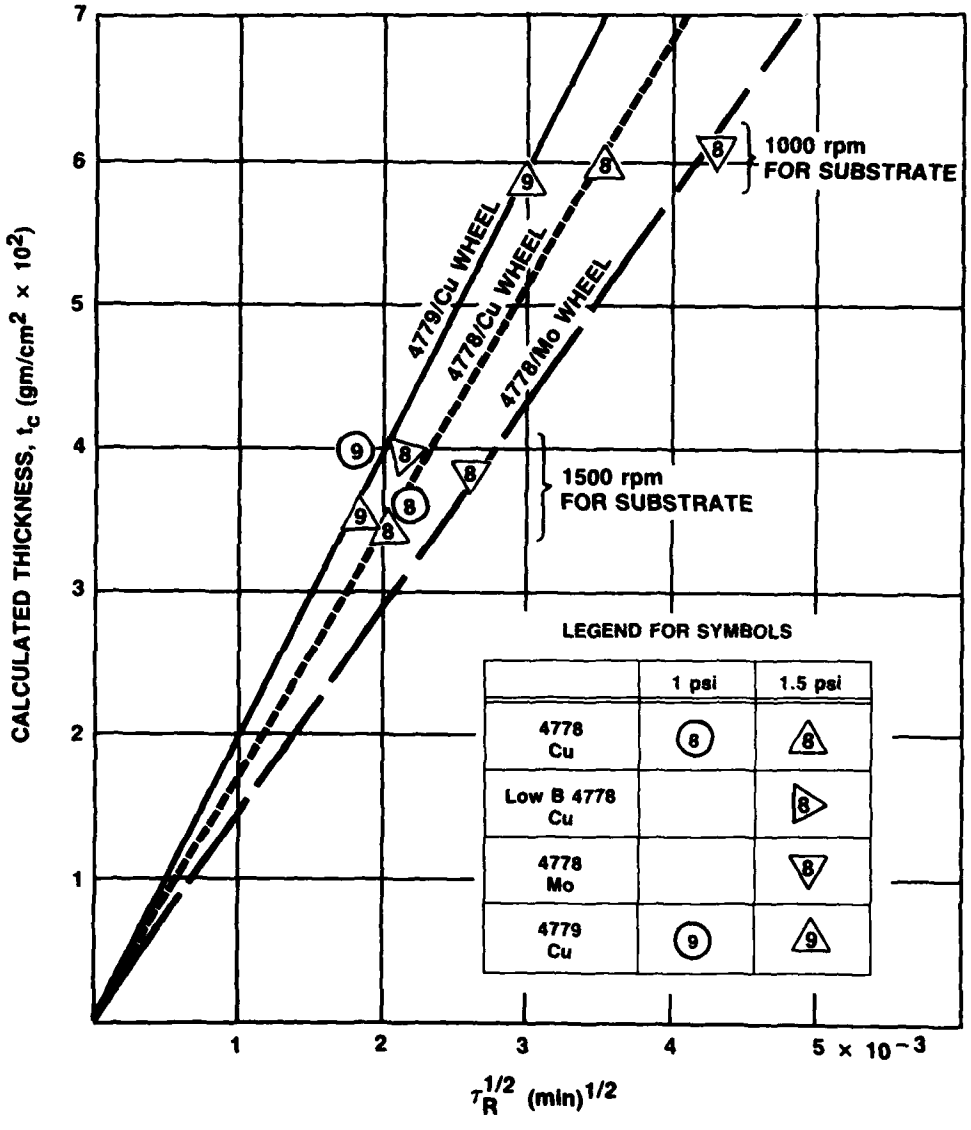

Figure 5. Solidification Kinetics

4.2 PHASE 2: EVALUATION OF CHANGES IN MELT CHEMISTRY

4.2.1 Objectives and Special Conditions

The objective of this phase of the program was to examine what changes in process and product characteristics occurred when melts with systematically varied compositions were melt spun. The baseline composition chosen was the ternary, deep eutectic Ni-base/ metalloid brazing alloy commercially available as AMS4778. AMS4778 with nominally 13 a/o B and 8 a/o Si, is a classic alloy that can be readily melt spun into a high quality amorphous product. The specific approach was to modify the boron level in this alloy so that at least some runs produced crystalline foils. By keeping the Si content (7.3 ± 1 a/o) relatively unchanged, the melting points of this series of alloys all fell within a reasonable range. In addition the synergistic effectiveness of B and Si in promoting amorphous foil formation could be varied by changes in the more active B component. Also a near eutectic Ni-B binary alloy was prepared so that one system without silicon could be evaluated. This compositional array of alloys (Table 5) was designed to allow us to separate and quantify the effects of B and Si on the melt spinning phenomenon as well as the quality and structure of the resultant product. The emphasis on boron content arises because the addition of this solute has been almost universally found to improve the melt spin processability of many alloys.

All prealloyed wire bar casting ingots were prepared by the Wesgo Division of GTE Products Corporation in Belmont, CA, following the same proprietary procedures as used for their commercially available Ni-base brazing alloy line. High purity Ni, Si and a Ni-B master alloy feedstock were vacuum induction melted and cast into 1 in. diameter bars from which nominally 100 gm sections were used for melt spinning runs. This practice assured that a consistent and reproducibly processed set of melt stock alloys were available.

Similarly a consistent set of previously described laboratory preparation and melt spinning procedures were maintained to allow cross comparisons with other sets of experimental results where either different substrate materials or other melt compositions were the major process parameter variables. High speed motion pictures were analyzed to quantify puddle phenomena (Table 5) and sample characterization provided dimensional, gravimetric, structural and morphological data (Table 6).

For this series substrate conditions were fixed by using our regular water cooled copper substrate rotating at 1500 rpm. The melt delivery system was a quartz pressure vessel with a 1 mm orifice through which the melt jet emerges when a 1.5 psi forming gas overpressure is applied.

4.2.2 Results and Discussion

Data for process and puddle characteristics for each melt spinning run were recorded in Table 5. In addition the foil residence time on the wheel was determined by measuring the circumferential contact arc length between the point of jet impingement and that of foil/wheel separation using a protractor mounted behind the wheel (from the observer). At a fixed 1500 rpm substrate rotation rate, each 9° arc angle is equivalent to a 0.001 second residence increment.

Data for foil characterization and quantitative values are listed in Table 5. Information from both Tables 5 and 6 represent stable processing conditions occurring after the initial revolution of the substrate but during the first three seconds of a run. Some run to run variations in the mass flow rate, as represented by the weight per unit length (W/L) values, are apparent but typically are accommodated by parallel changes in foil width. However the average calculated thickness (and to a lesser degree, the micrometer measured thickness values with their inherently larger scatter) remained constant (less than a 10% variation) with time as expected since substrate rotation rate was already shown to be the dominant parameter controlling foil thickness. Adjustments to short-term variations and the general long-term decrease in melt delivery rate are accommodated by changes in the height (note the larger coefficient of variation for the puddle height than for its length) and the width of the melt puddle and correspondingly the foil width. Thus the bulk averaged value of the calculated thickness is a useful parameter for correlating the systematic, second order run to run variations in puddle dynamics and solidification conditions due to deliberate changes in melt composition. Note that except for all but the two lowest boron containing melts the calculated thicknesses of 3.40 ± 0.15 are relatively insensitive to boron content. However the puddle contact length is proportional to boron content and essentially doubles from the low to the high end (Figure 6 which also includes earlier data for other alloy systems; starred symbols represent crystalline

TABLE 5

COMPARATIVE PROCESS VALUES FOR VARIABLE COMPOSITION SERIES WITH SIMILAR PROCESSING CONDITIONS**

SAMPLE IDENTIFICATION	ATOMIC PERCENT METALLOIDS		PUDDLE CHARACTERISTICS				FOIL/WHEEL CONTACT (ARC ANGLE IN DEGREES)
	% B	% Si	LENGTH* (mm)	HEIGHT* h (mm)	ASPECT RATIO h/ℓ	"AREA" $h \times \ell$	
Melt 42417	1.80	6.39	2.76 ± 0.6 (0.11)	2.60 ± 1.4 (0.27)	0.94	7.17	10 – 15°
Melt 42418	3.80	6.46	3.12 ± 0.84 (0.135)	2.82 ± 1.48 (0.263)	0.91	8.81	10 – 20°
Melt 42419	8.87	8.37	4.65 ± 1.16 (0.125)	2.02 ± 0.61 (0.153)	0.44	9.42	25°
Melt 42420	12.19	7.26	5.68 ± 1.42 (0.125)	2.12 ± 0.82 (0.193)	0.37	12.04	20 – 25°
AMS4778; "standard"	12.81	8.27	3.84 ± 0.79 (0.10)	2.79 ± 0.81 (0.15)	0.73	10.7	25 – 40° (estimated)
Melt 42416 "near eutectic binary"	14.43	0.33***	5.21 ± 1.13 (0.11)	2.0 ± 0.58 (0.15)	0.39	10.42	5 — 10°

*Measured statistics from high speed motion pictures typically from over 150 frames; variation range for mean value from 2σ (where σ is the standard deviation) thus only 4.6% of the measurements fall outside of this range; term in parenthesis is the coefficient of variation (σ/x).

**Melt ejected through 1 mm diameter orifice with 1 1/2 psi overpressure onto copper wheel rotating at 1500 rpm.

***Slight pickup of Si from melt delivery system.

TABLE 6

COMPARATIVE PRODUCT VALUES FOR VARIABLE COMPOSITION SERIES WITH SIMILAR PROCESSING CONDITIONS
(MELT EJECTED WITH 1.5 psi OVERPRESSURE THROUGH 1 mm DIAMETER ORIFICE ONTO A 1500 rpm COPPER WHEEL)

SAMPLE	ATOMIC PERCENT METALLOIDS		DIMENSIONAL VALUES				X-RAY EVALUATION	FOIL CHARACTERISTICS
	a/o B	a/o Si	WEIGHT PER UNIT LENGTH W/L (gm/m)	WIDTH w (mm)	THICKNESS t (mm)	CALCULATED THICKNESS* (W/L ÷ w)		
Melt 42417	1.80	6.39	0.633	1.45	0.058	4.36	Crystalline; primarily Ni-base fcc phase with trace of Ni_3B	Ductile; smooth edge profile with some width varicosity; few thru thickness voids; concave profile**
Melt 42418	3.80	6.46	0.771	2.01	0.056	3.82	Crystalline; primarily Ni-base fcc phase with minor amount of Ni_3B	Ductile (can be broken with repeated 180° bending); width varicosity with edge slivering and thru thickness voids; concave profile**
Melt 42419	8.87	8.37	0.582	1.80	0.048	3.26	Amorphous	Flexible; continuous lightly scalloped*** edges with occasional sliver; flat profile**
Melt 42420	12.19	7.26	0.765	2.16	0.053	3.55	Amorphous	Flexible; continuous very fine scale scalloped*** edges; flat profile**
AMS4778 "standard"	12.81	8.27	0.57	1.65	0.056	3.46	Amorphous	Flexible; continuous, occasional minor scallops on edges; flat profile**
Melt 42416	14.43	0.33	0.705	2.08	0.051	3.39	Crystalline; major phases of Ni-base fcc and Ni_3B with preferred orientation	Very brittle; straight edges without scalloping; concave profile**

*Units for calculated thickness values are 10^{-2} gm/cm².

**Transverse cross-sectional profile has either (1) a *concave profile* due to a shape change with foil edge sections curved away from the original substrate plane producing a *concave* free surface profile or (2) a *flat profile* where there was no shape change and the free and contact surface remain *flat*.

***Scalloped edge features indicative of some transverse puddle surface retraction during melt spinning.

foils). Corresponding average growth rates were calculated from the ratio of foil thickness to the residence time under the puddle. A growth rate range from a low of 150 mm/s for the Ni-B binary to a high of 355 mm/s for the lowest boron content alloy was found for this series of melts and the normalized values have been plotted in Figure 6. A similar analysis based on Si content produced no useful correlation.

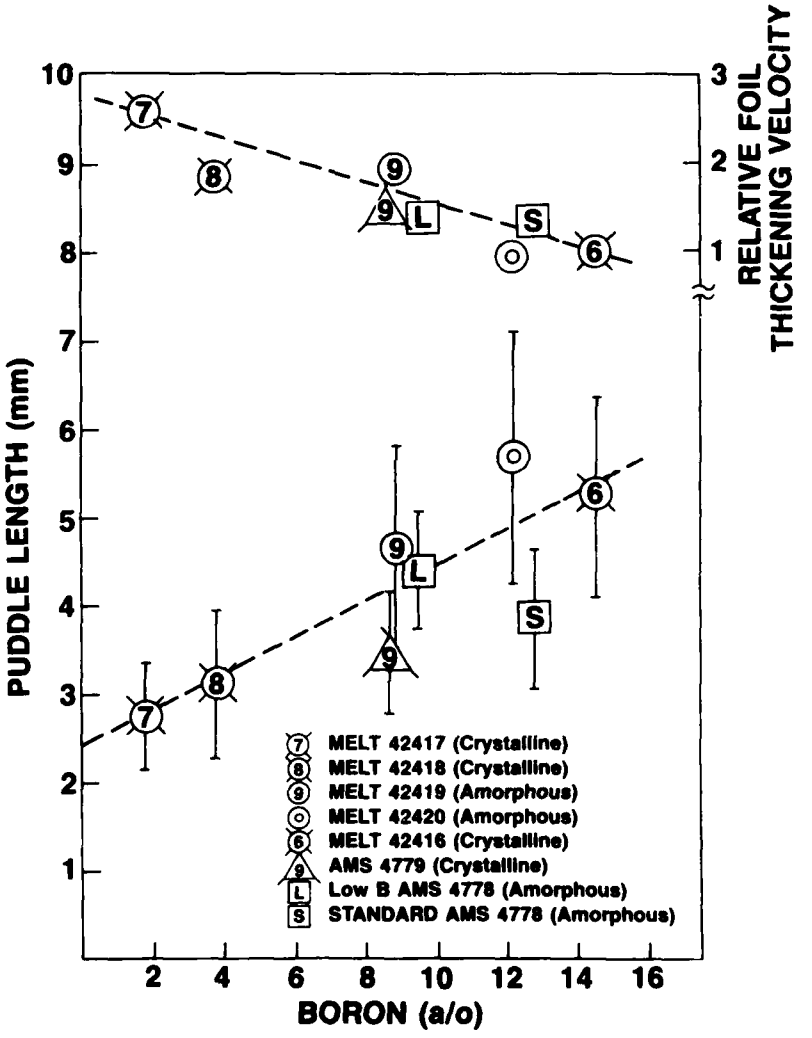

Figure 6. Variation of Puddle Length and Relative Foil Thickening Velocity with Boron Solute Content

Clearly the inverse relationship between thickening velocity and puddle length is a manifestation that puddle shape adjusts to maintain mass and thermal balance and is only indirectly a function of whether crystalline or amorphous solidification is occurring. For a given alloy the appropriate solidification mode that in fact becomes active is the one that can best match the interface velocity and cooling rate constraints of the overall system.

Thus for the lowest boron content alloy (Ni-1.80 a/o B-6.39 a/o Si), the presence of the supersaturated fcc Ni-base alloy phase indicates that this near congruent, first order phase transformation had matching kinetics. The presence of a steep thermal gradient resulting from a higher interface or solidification temperature and the higher heat conductivity through its own already solidified crystalline layer (as opposed to a similarly formed amorphous layer with a lower conductivity) assures that higher heat transmission rates can be maintained for this crystalline solidification mode. Further increases in boron content reduces the calculated liquid/solid interface velocity (Figure 6) by nearly half for either crystalline (indicated by starred symbols) or amorphous foils. Finally, rapid solidification of the near eutectic Ni-B binary alloy produces a columnar two-phase structure with preferred orientation. This indicates that a coupled growth process is occurring and a slower moving solidification interface can be expected.

Another beneficial effect of boron on puddle dynamics is that this solute forms a continuous, liquid B_2O_3 film over the melt puddle.[36] In the brazing trade this "self-fluxing" effect is known to help spreading, probably by lowering the surface tension of the melt. This effect must also more easily accommodate melt puddle elongation during melt spinning so that there is a steady state balance between the melt introduction rate and the foil solidification/removal rate. This is especially fortunate for melt spinning the higher boron alloys which have just been shown to require longer solidification times. With much less boron, such as the cases for the Ni-1.8 a/o B-6.39 a/o Si and Ni-3.8 a/o B-6.46 a/o Si alloys these shorter, high aspect ratio puddles with smaller profile areas ($h \times \ell$) as tabulated in Table 5 resulted in the least stable puddles which produced foils with some cosmetic surface defects as well as dimensional irregularities and discontinuities.

Finally, a correlation between relatively short foil/wheel contact distances (as measured by contact arc angles less than 20°) and shape changes for

the two low boron alloys and the Ni-B binary in Table 5 has been determined. Of all runs evaluated, only these three alloys had transversely curved cross-sectional shaped foils (referred to as a concave profile in Table 6) that also were crystalline. Thus normal volume shrinkage during crystalline solidification causes this foil shape change that promotes foil/wheel debonding. In all three cases this "premature" release combined with the extra thermal load created by the release of latent heat allowed these foils to leave the wheel still dull red hot. In contrast amorphous foils typically were much cooler since staying on the wheel longer allowed more conductive heat transfer.

4.3 *PHASE 3: EVALUATION OF ALTERNATE SUBSTRATE MATERIALS*

4.3.1 Objectives and Special Conditions

The objective of this phase of the program was to determine what changes in process and product characteristics occur when alternate substrate materials are used instead of copper. These included copper electroplated with either Cr or Ni, 1040 steel, 2024 aluminum and sintered Mo. This group of structural materials provide an opportunity to examine how pertinent substrate characteristics such as surface energy and heat transfer properties are for this form of dynamic wetting. Comparative values such as two thermal figures of merit and surface energy normalized relative to copper as well as melting points are listed in Table 1.

A limited array of commercially available ternary nickel-metalloid brazing alloys included AMS4779, AMS4778 and a modified, low boron AMS4778 (i.e., 9.4 a/o vs 12.8 a/o B in the regular alloy) were chosen because when melt spinning with a copper wheel metalloid lean melts form crystalline foils while higher metalloid melts form amorphous foils. In addition Ni-base AMS4777 (with 14.7 a/o B, 7.1 a/o Si, 2.7 a/o Fe, and 6.7 a/o Cr) provided an opportunity to evaluate whether the presence of an element common to both the melt and the surface of the wheel had any significant impact on the dynamic wetting process[37-39] occurring during melt spinning. All of these alloys were prepared according to proprietary procedures at the Wesgo Division of GTE Products Corporation.

Typically 100 gm bar sections were melt spun into samples using previously described laboratory preparation, melt spinning and analytical proce-

dures. Data for puddle and process phenomena are listed in Table 7 and sample characteristics are tabulated in Table 8.

4.3.2 Results and Discussion

Characteristics for the puddle dynamics and process features for each melt spinning run with various combinations of melt and substrate material are listed in Table 7. Puddle length varied by a factor of two. The order of plotting data in Figure 7 started with copper followed by substrate materials with increasingly greater puddle lengths. This order does not directly correspond with any of the surface energy or thermal figures of merit listed in Table 1. Using these concepts it is hard to rationalize why Al and Mo substrates produced the longest melt puddles but this will be subsequently explained.

The duration of foil/wheel contact (or the contact time at 1500 rpm) measured from the arc angle (Table 7) can be reasonably correlated with the inverse of the thermal diffusity figure of merit. One mechanism could be that foil release from the wheel takes place after a specific drop in interface temperature downstream of the puddle. This concept is consistent with our prior experience as well as that of others[19] that wider melt spun ribbons tend to have longer wheel contact lengths than narrower products. The additional heat release during wider tape melt spinning puts a greater thermal demand on the quenching subsystem. Thus the surface temperature of the substrate takes longer to return to its minimum baseline value.

The increase of the foil/wheel contact length based on common element considerations has been found to be selective rather than universal. For each alloy melt compared to values from a copper wheel (Table 7), only Fe (in AMS4777) could be shown to increase the contact length on an Fe wheel. For Cr (also in AMS4777), a similar extension of the contact length on the Cr plated wheel was only marginal. In contrast for all these Ni-base alloys there was no or even a slight negative effect on the contact length when the Ni-plated wheel was used. Since this phenomenon empirically appears to be selective, any explicit relationship most probably is masked by other more dominant phenomena.

Characterization of the dimensional values and other foil features for the various combinations of melt and substrate has been summarized in Table 8.

TABLE 7

COMPARATIVE PROCESS VALUES FOR VARIABLE SUBSTRATE/MELT SERIES WITH SIMILAR PROCESS CONDITIONS*

MELT	SUBSTRATE	PUDDLE CHARACTERISTICS				FOIL/WHEEL CONTACT (ARC ANGLE IN DEGREES)
		LENGTH** ℓ (mm)	HEIGHT** h (mm)	ASPECT RATIO h/ℓ	"AREA" h x ℓ	
AMS4779	Cu	3.47 ± 0.72	2.47 ± 0.80	0.71	8.58	10 - 15° (E)
Low B	Cu	4.39 ± 0.66	1.83 ± 0.46	0.42	8.03	25 - 35°
AMS4778	Fe	4.76 ± 1.30	1.65 ± 0.32	0.35	7.85	25 - 40° (E)
	Ni/Cu	5.02 ± 0.91	1.57 ± 0.27	0.31	7.86	15°
	Cr/Cu	5.70 ± 1.60	1.51 ± 0.50	0.27	8.59	20°
AMS4778	Cu	3.84 ± 0.79	2.79 ± 0.81	0.73	10.7	25 - 40° (E)
	Mo	6.31 ± 1.96	1.99 ± 0.78	0.32	12.56	60 - 90° (E)
AMS4777	Cu	4.62 ± 1.30	2.26 ± 0.70	0.49	10.43	25 - 30°
	Fe	4.84 ± 0.62	2.35 ± 0.50	0.49	11.35	65°
	Ni/Cu	3.89 ± 0.30	1.78 ± 0.30	0.46	6.92	20 - 30°
	Cr/Cu	5.16 ± 0.74	1.87 ± 0.38	0.36	9.63	35°
	Al	6.38 ± 1.35	1.84 ± 0.61	0.29	11.74	35°

*Melt ejected through 1 mm diameter orifice with 1.5 psi overpressure onto a substrate wheel rotating at 1500 rpm.
**Measured statistics from high speed motion pictures typically over 150 frames; variation range for the mean value from 2 σ limits (where σ is the standard deviation) thus only 4.6% of the measurements fall outside of this range.
(E) Estimate only.

TABLE 8

COMPARATIVE PRODUCT VALUES FOR VARIABLE SUBSTRATE/MELT SERIES WITH SIMILAR PROCESSING CONDITIONS**

MELT	SUBSTRATE	DIMENSIONAL VALUES				FOIL CHARACTERISTICS
		WEIGHT PER, UNIT LENGTH, W/L (gm/m)	WIDTH, w (mm)	THICKNESS, t (mm)	CALCULATED THICKNESS* (WL/ + w)	
AMS 4779	Cu	0.72	2.06	0.062	3.48	Crystalline; minor edge scalloping,*** longitudinal array of contact surface voids; lightly oxidized free surface.
Low B AMS 4778	Cu	0.75	1.85	0.058	4.04	Amorphous with some fcc phase; good quality with no edge scalloping.
	Fe	0.484	1.21	0.056	3.78	Crystalline; infrequent edge scalloping, contact surface has finer voids often in linear array — may be associated with substrate grooves.
	Ni/Cu	0.504	1.35	0.056	3.77	Crystalline with a trace of amorphous phase; edges with occasional scallop; contact surface is excellent substrate replica with very few voids.
	Cr/Cu	0.455	1.21	0.056	3.60	Crystalline; continuous light scalloped edges, contact surface has random pattern of voids.
AMS 4778	Cu	0.57	1.65	0.056	3.46	Amorphous; infrequent edge scalloping, good quality continous product.
	Mo	0.73	2.03	0.069	3.82	Amorphous to crystalline — as wheel heats up during run; foils get narrower, more crowned and scalloped.
AMS 4777	Cu	0.674	1.83	0.056	3.71	Amorphous; continuous foil with scalloped edges; free surface protrusions; contact surface has large and small voids.
	Fe	0.505	1.52	0.061	3.45	Amorphous; continous foil with scalloped and slivered edges; contact surface replicates wheel and has large voids.
	Ni/Cu	0.54	1.40	0.060	3.70	Amorphous; continuous foil with scalloped and slivered edges; contact surface replicates substrate linear features.
	Cr/Cu	0.57	1.78	0.056	3.27	Amorphous; continuous with very heavy edge scalloping; contact surface has large voids.
	Al	0.619	1.75	0.053	3.41	Amorphous; continuous foil with scallops and slivers; contact surface with voids some interconnected.

*Units for calculated thickness values are 10^{-2} gm/cm².
**Melt ejected through 1 mm orifice with 1.5 psi overpressure onto substrate wheel rotating at 1500 rpm.
***Scalloped edge features indicative of some transverse puddle surface retraction during melt spinning.

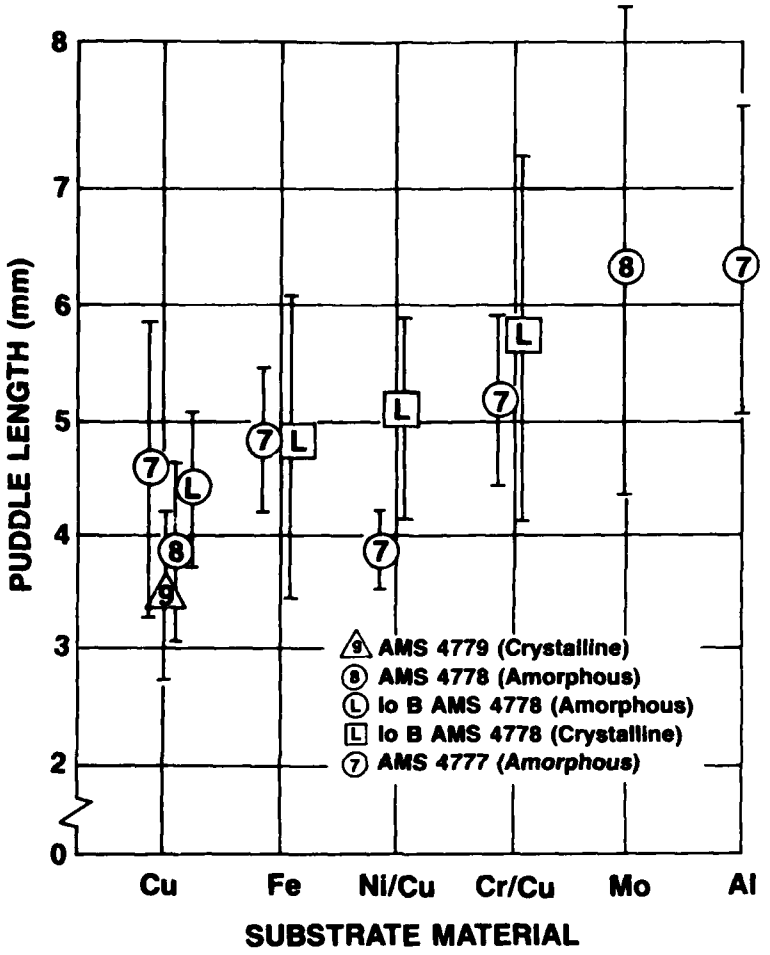

Figure 7. Variation of Puddle Length for Copper and Alternate Substrate Materials

Some run to run variations in mass flow rate are apparent from the weight per unit length values, but these are generally matched by the equivalent change in width. As reasoned previously the calculated thickness values will again be used to make systematic comparisons to help identify those second-order factors that affect the system and its products.

Analogous to the variable boron chemistry series, the magnitude of the puddle length did not correlate well with the calculated foil thickness which were typically between 3.4 and 3.8. The average foil thickness growth rates were similarly calculated. Growth rates ranged from a low of 133 mm/s for the AMS4777 melt/Al wheel combination which produced amorphous foil to a high of

284 mm/s for the AMS4779/Cu combination which made fully crystalline foils. Normalized values with respect to the AMS4778/Cu substrate combination are plotted in Figure 8. Comparing Figures 7 and 8, the inverse relationship between puddle length and foil thickening rate is evident. Thus once again puddle length is shown to be a flexible puddle feature that adjusts to the thermal and mass balance constraints for each system in operation.

Although the empirical ranking of the Fe wheel data between those for Cu and Ni plated onto Cu wheels in Figures 7 and 8 is somewhat subjective, the similarity of the processing characteristics for the Fe wheel to both the Cu and the Ni plated Cu wheels was unexpected based on either thermal figure of merit (Table 1). Comparative observations of the foil contact surface morphology (Table 8) indicate that the relative melt/substrate intimate contact area is typically less than 100%. The Ni-plated and the Fe wheels seemed to produce foils that had fewer voids and more faithfully replicated the substrate surface finish. At the other extreme the contact surface from foils made from the Mo wheel had a larger number of small and large voids; foils made on the Al wheel had contact surfaces with extensive, frequently interconnected void patterns that drastically reduced the actual melt/substrate contact area in both cases.

Another probable compounding factor is the presence of a tenacious oxide layer on the Cr and Al interfaces that could be expected to further reduce heat transfer rates across the foil/wheel interface in two ways. The oxide layer becomes a direct and additional resistive barrier to heat flow. Secondly as the surface energy of substrate interface is reduced by the formation of an oxide, there is an indirect but reduced tendency for the melt to wet the substrate as effectively.[37-39] Thus both mechanisms can reduce the magnitude of the rapid solidification rate.

Overall for these kinds of Ni-base alloys, copper still appears to be the best substrate material. Even thin electroplated layers of Ni or Cr seem to reduce the thermal transport rate compared to a bare copper quenchant subsystem. The resulting product tends to be narrower and have more pronounced edge scalloping, both features of a diminished rate of solidification during melt spinning. When more intimate melt contact was achieved as for the cases of two melt spinning runs with an Fe wheel and one with the Ni-plated wheel, the effective heat transfer rate was noticeably improved beyond that expected from

the thermal figures of merit. Thus Figure 8 can also be viewed as a measure of the relative interface heat transfer coefficient for the wheels being examined.

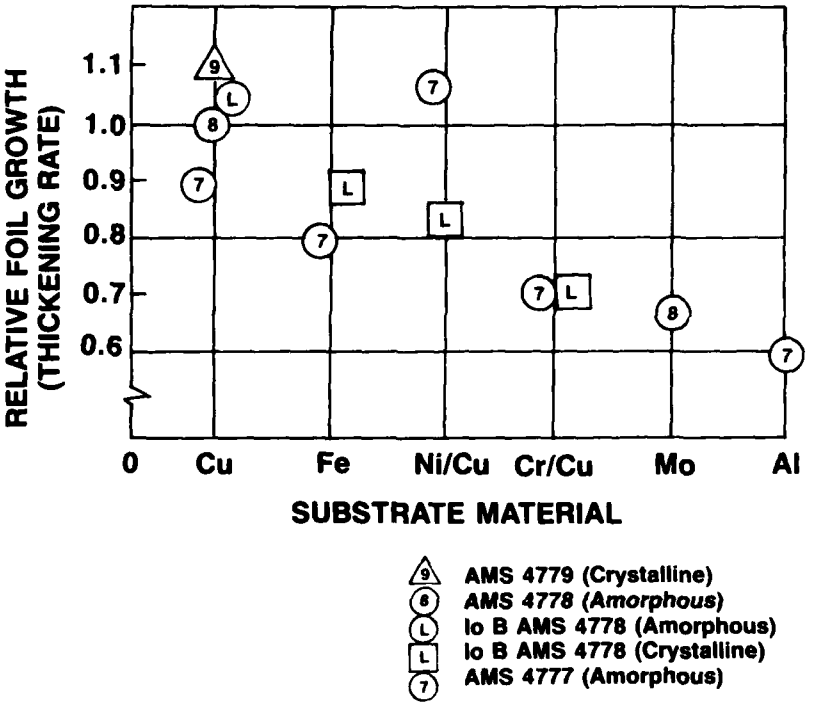

Figure 8. Relative Foil Thickening Rate During Solidification Under Melt Puddle for Copper and Alternate Substrate Materials

The use of an Fe substrate can be recommended for melt spinning amorphous products if the minimum or critical quench rate for that alloy system is not too high such as for the AMS4778 and 4777 alloys. On the other hand lower metalloid content alloys, such as the experimental low boron AMS4778 alloy, have higher critical quench rates for amorphous state retention. Thus when melt spinning with an Fe wheel the nominal 20% reduction in interface heat transfer coefficient (extrapolated from Figure 8) will slow down the heat transfer rate sufficiently that the amorphous state will not be fully retained. Even foils of this alloy melt spun on Cu have an estimated crystalline content (Table 9) in the 10% to 25% range, while a similar alloy product melt spun on Fe produces a fully crystalline foil.

Table 9 represents the results of a semiquantitative analysis for determining the crystalline/amorphous phase ratio. For this low B alloy, foils melt spun on Cu, Fe, and Ni- or Cr-electroplated Cu wheels were examined by x-ray diffraction techniques. Using Cu Kα radiation, diffraction traces between 60° and 20° 2θ were recorded. Quantitative values were based on measurements of the integrated area A(111) under the (111) fcc peak for the Ni-base solid solution phase (taken above the background radiation level or above the amorphous hump profile) as well as the integrated area A(a) of the first diffuse amorphous hump above the background radiation level. Two ratios were calculated. One, the normalized A(111) value compared to a reasonable but arbitrary value of 2100 (counts °2θ) was the more direct method. However it was subject to sample to sample and random equipment variations (estimated at up to ±20%; note that for the two different samples that were judged to be 100% crystalline the A(111) integrated areas were 2443 and 1851). The second method is more internally self-consistent since it ratios A(111) against the sum of A(111) and A(a) making this term independent of instrumental or sampling errors. However it is most likely that this ratio underestimates the absolute percent crystallinity especially when the value of A(111) is quite small. For our purposes the value for estimated percent crystallinity was taken from the weighted average of both terms.

What should also be noted for the foil melt spun on the copper wheel is that there were significant differences in the degree of crystallinity on the free and contact surfaces. One rationalization is that the surface layer of the foil adjacent to the substrate must be exposed to temperatures between the "solidification" and the crystallization values for a proportionately longer period of time while the rest of the overlaying elements, especially the free surface layer, solidify. Thus there is slightly more time for in situ crystallization to occur on the contact surface especially when the critical quench rates are relatively higher than the easy-to-melt-spin alloys that form amorphous foils. Since the rest of the results in Table 9 were obtained from the free surface side, the listed values particularly for the foil made on the Ni-electroplated wheel would represent a lower bound estimate of the actual amount of crystalline phase present.

These results indicate that the evaluation of both sides of melt spun foils using x-ray diffraction techniques could be a useful method for characterizing the structural state of melt spun products. In conjunction with

TABLE 9

X-RAY ANALYSIS FOR CRYSTALLINE/AMORPHOUS RATIOS IN LOW BORON AMS4778 MELT SPUN ON VARIOUS SUBSTRATES

RUN ID AND SUBSTRATE	SAMPLE SURFACE EXAMINED	PEAK HEIGHT* (111) fcc	INTEGRATED AREA VALUES				ESTIMATED CRYSTALLINITY FROM WEIGHTED AVERAGE OF A(111)/2100 AND A(111)/[A(a) + A(111)]
			AMORPHOUS HUMP, A(a)	(111) fcc PEAK, A(111)*	NORMALIZED** A(111)/2100	$\frac{A(111)}{A(a) + A(111)}$	
2/28/84 Cu	free surface	1130	3700	341	0.162	0.084	~10%
	contact surface	2090	2912	890	0.423	0.234	~25 – 35%
2/6/84 Fe	free surface	7696	0	2443	≈1	1.0	crystalline
2/7/84 Ni/Cu	free surface	3072	488	1131	0.539	0.699	~70%
2/3/84 Cr/Cu	free surface	4041	0	1851	≈1	1.0	crystalline

*Peak height or area taken above background level or above profile of the broad amorphous hump.

**For standardized x-ray conditions and uniform irradiated foil area, a fully crystalline AMS4778 foil was arbitrarily assigned a (111) integrated area intensity value of 2100 counts 2θ (for 2s count interval with 0.05° 2θ steps).

proper diagnostics and a melt quenching subsystem where the heat transfer rates can be systematically varied, it should be possible to quantify values for the critical amorphous/crystalline quench rate for many alloy systems.

5. CONCLUSIONS

This experimental program has investigated the dynamic phenomenology of melt spinning in order to understand the effects that process controls and material selection have on melt puddle characteristics which in turn influence the geometry and properties of melt spun products. In doing so a statistically significant number of quantitative measures of the melt puddle shape and dimensions were taken over periods of time where steady state conditions could be reached at least in the case when a water cooled copper substrate was used. As a result of this study and other useful publications[8, 11–13, 15, 21, 23] relating processing with product geometry, the following guidelines relating product dimensions with process variables [Table 10(a)] and puddle dynamics with puddle features [Table 10(b)] have been compiled.

Our results still indicate that Cu is the best substrate material for Ni-base alloys especially if the critical cooling rate to retain an amorphous structure is very high. An additional benefit is that the melt puddles on the Cu wheels tend to be more compact and oscillate less; this in turn improves dimensional uniformity of the product. The use of Cu electroplated with Ni or a solid Fe wheel is acceptable whenever the critical cooling rate to retain an amorphous foil from a given melt is not too high or when microcrystalline or crystalline products are desired. Also in special cases when longer foil/wheel contact arcs are desired and if the melt contains some Fe solute, this may be accomplished using an Fe wheel.

While neither solid Fe or Cu electroplated with Ni can match the bulk thermal transport properties of Cu, very good wheel interface contact with the solidifying foil occurs. Thus significant heat transfer rates can occur because the percent effective contact area is very high. For Cr plated Cu and Al wheels, experimental results and foil quality are less than expected. In part this has been attributed to the formation of a tenacious oxide film that decreases the tendency of the wheel peripheral surface to be wet by the melt. This is supported by a macroexam of contact surfaces of foils melt spun from Al or Cr plated wheels where the surface density of voids is higher than usual. The oxide film also acts as an additional thermal flow resistance barrier. Both factors reduce the bulk heat flow rate which causes puddle length extension. Reduced heat transfer rates and more extensive wetting of

TABLE 10

PROCESSING GUIDELINES

(a) Variations in Jet Velocity (V_j) and Substrate Velocity (V_s)

PRODUCT PARAMETER	VARIABLE	RELATIONSHIP	COMMENTS
Foil Width (w)	V_j	$w \propto V_j^n$ (exponent $n = 1 \pm 0.2$)	*Momentum* dominating effect
	V_s	As V_s increases, periodic width oscillations occur (both *varicosity* frequency and amplitude increase with V_s	*Mass Flow Rate* effect (continuous melt puddle size adjustment of lateral dimension)
		As V_s drops, more systematic *lateral puddle contraction* produces a foil that is thicker and narrower with increasingly more ragged edge definition	Due to decrease in effective localized heat removal rate, *surface tension* driven lateral contraction of the extended, still molten puddle occurs
Foil Thickness (t)	V_j	Thickness virtually independent of V_j	
	V_s	$t \propto R\, V_s^{-1/2}$ Where R weakly dependent on solidification mode and inversely on the thermal conductive properties and average temperature of the wheel	

(b) Puddle Dynamics

PROCESS PARAMETER	VARIABLE	RELATIONSHIP	COMMENTS
Puddle Length (ℓ)	General	Puddle length adjusts to solidification kinetics as controlled by thermal properties of substrate and melt	At arbitrary V_s, $\ell \propto R^{-1}$
Puddle Stability	Aspect Ratio, h/ℓ	Stable puddles with intermediate aspect ratios, $1/3 < h/\ell < 1$, have lower coefficients of length variation, $\triangle\ell/\ell$	Taller or longer puddles are inherently more unstable producing poor quality product

the higher surface energy Mo substrate by the melt produced the extended puddle length and contact surface porosity when a Mo wheel was used. When the higher mechanical properties of Mo or Fe relative to Cu are required, such substrates must be designed to have a superior internal coolant heat absorption capacity to avoid a significant rise in baseline wheel temperature. Otherwise degradation of foil quality will occur during long-term melt spinning production runs.

Changes in metalloid content have been used to demonstrate that melt puddle dynamics are only indirectly affected by the nature (e.g., amorphous vs crystalline) of solidification. For low metalloid concentrations, especially of B, melt spinning produces crystalline supersaturated Ni-base alloys where the puddle length is short because the solidified crystalline layer must have a higher thermal conductivity than its amorphous counterpart. Further increases in boron produced a longer puddle and amorphous foils were formed. For the highest boron content alloy a rather long puddle was needed to accommodate the relatively slow coupled growth interface velocity that produced a two phase columnar structure. Another important benefit of the boron solute is on puddle dynamics. The formation of a liquid B_2O_3 film over the melt puddle helps stabilize the puddle and improve puddle/substrate wetting. This is especially useful for many alloys that require a relatively long puddle to complete solidification. When melt spinning becomes difficult it is usually due to lack of puddle stability, therefore the addition of small amounts of boron can cause significant improvements.

An x-ray diffraction technique developed during this program to characterize the amorphous/crystalline state of melt spun foils appears to have merits in quantifying such results. For instance, evidence was developed indicating that the contact and free surfaces of foils could have different amounts of amorphicity/crystallinity. These diagnostic capabilities coupled with a melt quenching subsystem where effective heat transfer rates can be systematically varied might prove useful in quantifying the magnitude of the critical quench rate for a given material. This interesting topic could be the subject of another ONR sponsored research task.

An operational model of the melt spinning process can now be constructed which relates the relative influence of mechanical forces, surface energy, and heat transfer rates. The basic elements are a continuous compact liquid stream

that impinges on a moving, heat absorbing surface where the liquid may spread into a film with extended area if the mechanical forces initially exceed the net increase in surface energy forces. High quality melt spun product can be formed when the liquid stream forms a continuous thin film strip on the moving substrate but only if the heat transfer rate into the solid heat absorbing interface is high enough to solidify the liquid strip into a continuous foil with straight parallel sides. The system is usually forgiving so that a window of processing variables exists where desirable quality foil can be produced. Certain boundary conditions exist which define the limits of this processing window in relative terms:

1. One boundary condition occurs whenever the momentum forces in the stream are too low to cause liquid spreading on the substrate in a thin enough layer for solidification to take place. This situation has been reported[34] for the case of a low velocity stream which degenerated into droplets and short irregular fibers.

2. Another condition occurs when the substrate has or develops an effective heat transfer rate that is too low for complete solidification to occur. In this case the outspread film can partly (if some solidification occurs) or totally collect itself. Such occurrences have been reported:

   a) When much lower than optimal substrate rotation rates are used causing the formation of droplets.[27]

   b) When slightly lower than optimal substrate rotation rates are used so that partial retraction of the film occurs producing foil widths that are less than the transverse puddle diameter (e.g., foils melt spun at 1000 rpm are narrower than those formed at 1500 rpm - other factors being equal).

   c) Or when the heat transfer capacity of the substrate systematically decreases due to the formation of a thermal barrier layer at the original melt-substrate interface or from an increase in the baseline temperature of the wheel during a run (e.g., at a given rpm foils melt spun on Mo wheels are narrower at the end of the run).

3. The third boundary condition occurs when the stream velocity is so high that the extended and spreading film itself breaks up into separate fragments (such as during spinning disk atomization).

In overview, melt spinning should be considered as a steady state process where equilibrium concepts such as isothermal wetting cannot be directly applied. Instead control of dynamic forces and maintenance of an efficient and stable heat removal capacity by the substrate wheel are very important if a rapidly solidified product is to be continuously produced. When the process is operating properly, surface energy of the melt has only a secondary effect and only when the process falls out of its optimal operational window does surface energy exert a significant and often deleterious effect.

6. REFERENCES

1. R.B. Pond, U.S. Patent #2,825,108, "Metallic Filaments and Method of Making Same" (March 4, 1958).

2. R. Ray, C.F. Cline, D.E. Polk and L.A. Davis, U.S. Patent #4,154,283, "Production of Improved Metal Alloy Filaments" (May 15, 1979).

3. N. Tsuya and K. Arai, U.S. Patent #4,257,830, "Method of Manufacturing Magnetic Material" (March 24, 1981).

4. N. Tsuya and K. Arai, U.S. Patent #4,265,682, "High Silicon Steel Thin Strips and a Method for Making Same" (May 5, 1981).

5. M.C. Narasimhan, U.S. Patent #4,142,571, "Continuous Casting Method for Metallic Strips" (March 6, 1979).

6. K. Esashi and H. Minatono, U.S. Patent #4,337,087, "Microcrystalline Thin Strip for Magnetic Material Having High Permeability, a Method of Producing the Same and Articles Made from the Thin Strip" (June 29, 1982).

7. H.R. Hilzinger, K. Kruger and S. Hock, U.S. Patent #4,386,648, "Method and Device for Manufacture of Amorphous Metal Tapes" (June 7, 1983).

8. S. Kavesh, "Principles of Fabrication," Metallic Glasses, J.J. Gilman and H.J. Leamy editors, American Society for Metals, Metals Park, OH, pp. 36-73 (1978).

9. D.C. Agrawal, "Melt Spinning Parameters and the Geometry of Metallic Glass Ribbon," J. Mat. Sci. Lett. 1, pp. 385-386 (1982).

10. J.H. Vincent, J.G. Herbertson, and H.A. Davis, "Comments on the Geometry of Melt Spun Ribbon," J. Mat. Sci. Lett. 2, pp. 88-90 (1983).

11. H. Hillman and H.R. Hilzinger, "On the Formation of Amorphous Ribbons by the Melt Spin Technique," Rapidly Quenched Materials III, Proc. 3rd Intl. Conf. on Rapidly Quenched Metals, B. Cantor editor, The Metals Society, vol. 1, pp. 22-29 (1978).

12. H. Jones, "Review: The Status of Rapid Solidification of Alloys in Research and Application," J. Mat. Sci. 19, pp. 1043-1076 (1984).

13. D. Pavuna, "Production of Metallic Glass Ribbons by the Chill-Block Melt-Spinning Technique in Stabilized Laboratory Conditions," J. Mat. Sci. 16, pp. 2419-2433 (1981).

14. T.R. Anthony and H.E. Cline, "On the Uniformity of Amorphous Metal Ribbon Formed by a Cylindrical Jet Impinging on a Flat Moving Substrate," J. Appl. Phy. 49 (2), pp. 829-837 (1978).

15. T.R. Anthony and H.E. Cline, "Dimensional Variations in Newtonian-quenched Metal Ribbons Formed by Melt Spinning and Melt Extraction," J. Appl. Phys. 50 (1), pp. 245-254, (1979).

16. P. denDecker and A. Drevers, "Model Calculations on the Solidification and Crystallization Processes During Melt Spinning," Proc. Conf. on Metallic Glasses: Science and Technology 1, pp. 181-188, C. Hargitai, I. Bakonya and T. Kemeny editors, Central Research Institute for Physics, Budapest (1980).

17. R.P.I. Adler and S.C. Hsu, "Dynamic Processing Characteristics for Melt Spinning," Rapidly Solidified Metastable Materials, B.H. Kear and B.C. Giessen editors, Elsevier Science Publishing, 1984, (in press).

18. S. Tomita and H. Suzuki, "The Relation between the Process Conditions and Shape of Amorphous Metal Ribbons Fabricated by the Single Roll Method," J. Japan Inst. Metals 48 (2), pp. 202-208 (1984).

19. H.R. Hilzinger and S. Hock, "Preparation of Metallic Glasses," ibid Ref. 16, pp. 71-90.

20. S.J.B. Charter, D.R. Mooney, R. Cheese and B. Cantor, "Melt Spinning of Crystalline Alloys," J. Mat. Sci. Lett. 15, pp. 2658-2661 (1980).

21. F.E. Luborsky, H.H. Liebermann and J.L. Walter, "The Effect of Ribbon Thickness, Composition and Process Changes on the Properties of Rapidly Quenched Metal-Metalloid Alloys, ibid Ref. 16, pp. 203-214.

22. H.H. Liebermann, "Helical Glassy Alloy Ribbons: Fabrication and Magnetic Properties," Mat. Sci. Eng. 49, pp. 185-191 (1981).

23. H.H. Liebermann, "The Dependence of the Geometry of Glassy Alloy Ribbons on the Chill Block Melt Spinning Process Parameters," Mat. Sci. Eng. 43, pp. 203-210 (1980).

24. F.E. Luborsky and H.H. Liebermann, "Effect of Melt Temperature on Some Properties of $Fe_{80.5}$ B_{15} Si_4 $C_{0.5}$ and Fe_{40} Ni_{40} B_{20} Amorphous Alloys," Mat. Sci. Eng. 49, pp. 257-261, (1981).

25. H.H. Liebermann, "Coaxial Jet Melt Spinning of Glass Alloy Ribbons," J. Mat. Sci. 15, pp. 2771-2776 (1981).

26. H.H. Liebermann, "Manufacture of Amorphous Alloy Ribbons," IEEE Trans. of Magnetics Mag-15, 6, pp. 1393-1397 (1979).

27. H.H. Liebermann, "Gas Boundary Layer Effects in Processing Glassy Alloy Ribbons," ibid Ref. 11, pp. 34-40.

28. D. Pavuna, "On the Improvements of Metallic Glass Ribbons' Geometry - the Quenching Stabilizer," J. Non-Crystalline Solids 37, pp. 133-137 (1980).

29. M. Matsuura, M. Kikuchi, M. Yagi and K. Suzuki, "Effect of Ambient Gases on Surface Profile and Related Properties of Amorphous Alloy Ribbons Fabricated by Melt Spinning," Jap. J. Appl. Phys. 19, (9), pp. 1781-1787 (1980).

30. U. Koster, U. Herold, and H.G. Hillenbrand, "Influence of Solidification Parameters on Mechanical Properties and Thermal Stability of Fe-Ni-B Metallic Glasses," Scripta Metallurgica 17, pp. 867-872 (1983).

31. C.E. Mobley, R.E. Maringer and L. Dillinger, "Surface Features of Rapidly Quenched Filaments," Intl. Conf. Rapid Solidifcation Processing: Principles and Technologies, R. Mehrabian, B.H. Kear, and M. Cohen editors, Claitors Press, Baton Rouge, LA, pp. 222-229 (1977).

32. S.C. Huang and H.C. Fiedler, "Effects of Wheel Surface Conditions on the Casting of Amorphous Metal Ribbons," Met. Trans. 12A, pp. 1107-1112 (1981).

33. R.W. Smith, N.S. Hemmat, J.R. Bedell, S. Kavesh and S. Draizen, U.S. Patent #4,290,476, "Nozzle Geometry for Planar Flow Casting of Metal Ribbon" (September 22, 1981).

34. J.L. Walter, "A Study of the Formation of Amorphous Ribbon Using High-Speed Motion Pictures," ibid Ref. 11, pp. 30-33.

35. R.P.I. Adler and S.C. Hsu, "Dynamic Wetting/Solidification Phenomena," Proc. Third Conf. Rapid Solidification Processing; Principles and Technologies, R. Mehrabian editor, pp. 448-451 (1982).

36. CRC Handbook of Chemistry and Physics, 61st Ed., R.C. Weast editor, CRC Press, Boca Raton, FL p. B-84 (1980).

37. A. Bondi "The Spreading of Liquid Metals on Solid Surfaces," Chem. Rev. 52, pp. 417-458 (1953).

38. R.J. Klein Wassink, "Wetting of Solid Metal Surfaces by Molten Metals," J. Inst. of Met. 95, pp. 38-43 (1967).

39. J.V. Naidich and J.N. Churashov, "Wettability and Contact Interaction of Gallium Containing Melts with Non-Metallic Solids," J. Mat. Sci. 18, pp. 2071-2080 (1983).


ATE
LME